Influence of Baroclinic Eddies on the Hadley Cell Edge

SEUNGPYO LEE,[a] WOOSOK MOON,[a] SOOHYUN AHN,[a] SEOK-WOO SON,[b] AND KYONG-HWAN SEO[c,d]

[a] *Division of Earth Environmental System Sciences, Major of Environmental Atmospheric Sciences, Pukyong National University, Busan, South Korea*
[b] *School of Earth and Environmental Sciences, Seoul National University, Seoul, South Korea*
[c] *Department of Atmospheric Sciences, Division of Earth Environmental System, Pusan National University, Busan, South Korea*
[d] *Institute for Future Earth, Pusan National University, Busan, South Korea*

(Manuscript received 11 December 2024, in final form 17 August 2025, accepted 9 October 2025)

ABSTRACT: The Hadley cell (HC), a thermally direct circulation in the tropics, is known as the primary cause of tropical rainforest and subtropical desert formation. While its formation and maintenance have been extensively examined, the theoretical understanding of the dynamics governing its extent remains incomplete. The most fundamental theory on the HC considered the conservation of angular momentum and the energy constraint while neglecting the influence of baroclinic eddies. Held later considered the possible impact of baroclinic eddies and suggested that the HC edge is determined by the static stability and tropopause height at midlatitudes. By extending Held and Hou and updating Held, this study incorporates eddy heat fluxes and changes in adiabatic processes induced by eddy momentum fluxes into the energy flux balance in the HC. The updated energy flux balance shifts the latitude of the HC edge, depending on whether the heat exported by baroclinic eddies increases or decreases. This finding is verified through a series of idealized model experiments with varying baroclinicity.

SIGNIFICANCE STATEMENT: The Hadley cell (HC) is a major climate system component sustaining tropical rainforests and subtropical deserts. While pioneering work considered an isolated HC constrained by angular momentum conservation, Held highlighted the significant impact of baroclinic eddies at midlatitudes on HC dynamics. By explicitly establishing the theoretical effect of baroclinic eddies from the original HC model, this study provides a refined framework for understanding the role of baroclinic eddies in shaping HC dynamics.

KEYWORDS: Atmospheric circulation; Hadley circulation; Large-scale motions; Baroclinic flows

1. Introduction

Recent climate model simulations and reanalysis data show that as global warming progresses, the poleward edge of the Hadley cell (HCE) is shifting poleward (Nguyen et al. 2013, 2015; Kim and Son 2020; Lu et al. 2007; Grise and Davis 2020; Watt-Meyer et al. 2019; Fu et al. 2006). It is accompanied by a poleward shift in dry zones (Lu et al. 2007; Feng and Fu 2013), affecting regional precipitation patterns (Schmidt and Grise 2017; Rao et al. 2022) and altering cyclone activity (Studholme et al. 2022). A recent study further revealed that, under carbon dioxide (CO_2) mitigation scenarios, the HCE does not recover in the Southern Hemisphere, whereas it overly recovers in the Northern Hemisphere (Kim et al. 2023).

The Hadley cell (HC) and its edge have been theoretically understood through the work of Schneider (1977) and Held and Hou (1980; hereafter HH80). The pioneering HH80 model defines the HC by assuming the conservation of angular momentum as air parcels move from the tropics to the subtropics in the upper troposphere. The model simplifies the extratropics as an eddy-free region in radiative–convective equilibrium (RCE) and determines the HCE on the basis of a balance of diabatic processes in the tropics and subtropics. In other words, the HH80 model provides the basic dynamics of the HC under conditions of both momentum and energy conservation.

The real atmosphere clearly differs from the simplified assumption of the original model. In particular, baroclinic eddies at midlatitudes play a crucial role in mitigating the meridional thermal imbalance (Seo et al. 2014). Idealized model experiments have shown that the presence or absence of baroclinic eddies leads to substantial differences in the structure of the HC (Becker et al. 1997; Kim and Lee 2001). This finding indicates that the presence of baroclinic eddies can significantly modify the energy conservation constraint proposed in HH80 theory, thereby influencing the dynamics and extent of the HC.

Based on this understanding, alternative models incorporating baroclinic eddies have been proposed. Held (2000; hereafter H2000) noted that the upper-level flow of the HC conserves angular momentum only up to the latitude where baroclinic instability occurs. By combining this with the baroclinic instability criterion derived from a two-layer model (Phillips 1954), the width of the HC is scaled by subtropical static stability and tropopause height. Climate model simulations support this theory, revealing that changes in HC width depend more on the subtropical tropopause height than on its tropical counterpart (Lu et al. 2007). In another approach, Korty and Schneider (2008) proposed scaling based on supercriticality, defining the HCE as the latitude where the sign of the eddy angular momentum flux changes. The fact that angular momentum is not conserved in the upper subtropical region (Walker and Schneider 2006) and

Denotes content that is immediately available upon publication as open access.

Corresponding authors: Woosok Moon, woosok.moon@gmail.com; Kyong-Hwan Seo, khseo@pusan.ac.kr

DOI: 10.1175/JCLI-D-24-0705.1

that the real atmosphere is continuously stratified lends further support to this theory. These subsequent studies consistently suggest that baroclinic eddies play a key role in shaping the HC.

While H2000 provides a useful scaling for the HCE, the influence of baroclinic eddies was not derived from the thermodynamic framework of the original HH80 model. This presents a limitation in quantitatively assessing the impact of baroclinic eddies on HC dynamics. Therefore, developing a theoretical framework that explicitly links the tropics and extratropics within the HH80 model remains an important challenge. Moon and Wettlaufer (2025) approached this issue by extending the HH80 framework to include interactions between the HC and the extratropics. They employed a planetary-scale heat equation that parameterizes synoptic-scale eddies (Moon et al. 2021) and simplified the interaction between the two regions as eddy diffusion. Specifically, their model incorporates poleward heat transport—represented by eddy heat flux (EHF) near the HCE—into the energy flux balance. They proposed a mechanism in which the EHF governs the thermodynamic state of the HC, which, in turn, determines its structural characteristics. Their findings suggest that both the width and intensity of the HC scale with EHF: Weaker baroclinic eddies reduce poleward EHF at the HCE, resulting in increased temperatures within the HC and, ultimately, its expansion.

The present study builds upon Moon and Wettlaufer (2025) but improves their energy flux balance by incorporating the effects of adiabatic processes associated with eddy momentum flux (EMF) in the subtropical upper troposphere. The energy balance, by considering baroclinic eddies, can be summarized by three key components: 1) EHF at the HCE, 2) subtropical adiabatic warming (AW), and 3) tropical adiabatic cooling (AC). The proposed scaling of the HC is then evaluated by performing a series of dynamic core model experiments with varying degrees of baroclinicity.

Section 2 introduces the conventional energy flux balance for an energetically isolated HC, as formulated by HH80, and presents an updated energy flux balance that incorporates the influence of baroclinic eddies. This approach is combined with the thermodynamic approach of Moon and Wettlaufer (2025) to derive the physical role of baroclinic eddies. Section 3 introduces the dynamic core model and nine thermal forcing experiments and presents the definitions of the variables used in this study. Section 4 explains the eddy-induced thermal processes linking the HC and baroclinic eddies by connecting the theoretical developments in section 2 with the model experiments in section 3. The responses of both the HCE position and HC strength to baroclinic eddy activity are also discussed.

2. Theory

a. *HH80 model*

1) Momentum and energy conservation

The HH80 model considers the HC extending from 0 to ϕ_H (HCE latitude). It assumes that along the cell's circulation, an air parcel rises from the equator and moves to the upper HCE while conserving its angular momentum under inviscid conditions $\Omega a^2 = a\cos\phi(\Omega a\cos\phi + u_M)$, where Ω and a are Earth's rotation rate and radius, respectively. The upper-level zonal wind u_M conserving angular momentum from the equator is then derived and approximated using a small-angle approximation:

$$u_M = \Omega a\frac{\sin^2\phi}{\cos\phi} \approx \Omega a\phi^2. \tag{1}$$

The zonal-mean zonal wind is associated with the potential temperature via the thermal wind balance $2\Omega\phi(\partial u/\partial z) = -(g/a)(\partial\theta/\partial\phi)$, where P is the pressure and g is the gravity. Integrating the thermal wind balance vertically from the surface ($z = 0$) to the top of the atmosphere ($z = H$) leads to a relationship between the zonal wind and the meridional potential temperature gradient in the upper troposphere:

$$u(H) = -\frac{gH}{2\Omega\phi a}\frac{\partial\theta}{\partial\phi}. \tag{2}$$

Here, H represents the tropical tropopause height and θ represents the vertically averaged potential temperature. The $u(H)$ represents the zonal-mean zonal wind in the upper troposphere, which is assumed to be equal to u_M. By substituting Eq. (1) into Eq. (2) and integrating with respect to latitude, the potential temperature profile normalized by a reference potential temperature θ_0 can be derived as

$$\theta(\phi) = \theta_{\mathrm{eq}} - \frac{\Delta_H}{2R}\phi^4, \tag{3}$$

where θ_{eq} is an integration constant representing the potential temperature at the equator, Δ_H is the fractional potential temperature change from the equator to the pole in the RCE profile, and R is the thermal Rossby number, defined as $gH\Delta_H/\Omega^2a^2$. To close the model, two unknowns—θ_{eq} and ϕ_H—must be determined.

To solve these problems, two thermodynamic constraints are considered. First, the tropical circulation transports surplus heat from the equator toward the poles to compensate for the latitudinal thermal imbalance. This imbalance is based on the potential temperature profile determined by the RCE, which can be expressed as

$$\theta_E(\phi) \approx 1 + \frac{1}{3}\Delta_H - \Delta_H\phi^2. \tag{4}$$

Here, $\theta_E(\phi)$ represents the RCE potential temperature distribution. The tropical circulation redistributes $\theta_E(\phi)$, establishing a new potential temperature distribution $\theta(\phi)$ within the HC. The assumption that $\theta_E = \theta$ is outside the HC implies that there is no poleward heat transport by baroclinic eddies. In a steady state, the HC maintains an isolated energy flux balance, which HH80 expresses in terms of potential temperature conservation. Additionally, the potential temperature must be continuous at the HCE ($\phi = \phi_H$). Accordingly, the following two constraints are imposed on the HC:

$$\int_0^{\phi_H}\theta\,d\phi = \int_0^{\phi_H}\theta_E\,d\phi$$
$$\theta(\phi_H) = \theta_E(\phi_H). \tag{5}$$

Using these constraints, HH80 derives the HCE latitude under angular momentum and energy conservation as

$$\phi_H = \sqrt{\frac{5}{3}R} \propto \sqrt{H_t \Delta_H}. \tag{6}$$

This scaling indicates that the poleward edge of the HC is determined by the tropical tropopause height H_t and the fractional potential temperature difference Δ_H between the equator and the pole in the RCE.

2) TREATMENT OF BAROCLINIC EDDIES

H2000 proposed a new scaling for the HCE that accounts for the influence of baroclinic eddies. This scaling is based on an empirical conjecture suggesting that baroclinic eddies disrupt the conservation of angular momentum. Consequently, it is proposed that the HCE is determined by the latitude up to which angular momentum is conserved—specifically, up to the region where baroclinic instability arises. Using the baroclinic instability criterion derived from Phillips' two-layer model, the H2000 scaling can be expressed as

$$\phi_H \propto \sqrt{\frac{NH_e}{\Omega a}}, \tag{7}$$

where N is the static stability and H_e is the extratropical tropopause height. While this provides a useful empirical scaling for explaining the HCE, this formulation is not derived from a thermodynamic framework, such as an extension of HH80.

This study investigates the impact of baroclinic eddies on the HC within a more robust theoretical framework. Specifically, we examine the influence of baroclinic eddies from the perspective of energy flux balance in the HH80 model. Consider the heat equation $(d\theta/dt) = Q$, where Q represents radiative heating, expressed as $Q = -[(\theta - \theta_E)/\tau] = -(\eta/\tau)$. Here, τ is a radiative relaxation time scale associated with the sensitivity of the local radiative–convective process to temperature changes. Consequently, the steady-state, zonally, and temporally averaged thermodynamic energy equation becomes

$$\frac{\partial}{\partial \phi}\langle \overline{v'\theta'} \rangle + \langle \overline{Sw} \rangle = -\frac{1}{\tau}\eta, \tag{8}$$

where v and w are the meridional and vertical velocities, respectively, and S is the dry static stability. The $\cos\phi$, which appears in representing the divergence of the meridional heat flux in the spherical coordinate, is approximated as 1 under the small-angle approximation. The overbar and angle brackets denote the zonal and temporal means, respectively, and primes indicate the eddy components (i.e., deviations from the zonal mean).

By integrating Eq. (8) over the domain of the HC (from the equator to the HCE), we obtain

$$\int_0^{\phi_H} \frac{\partial}{\partial \phi}\langle \overline{v'\theta'} \rangle d\phi + \int_0^{\phi_H} \langle \overline{Sw} \rangle d\phi = -\frac{1}{\tau}\int_0^{\phi_H} \eta \, d\phi. \tag{9}$$

In this equation, the first term on the left-hand side represents the EHF at ϕ_H and the second term corresponds to the total adiabatic processes within the HC. The right-hand side represents the radiative cooling (or heating) integrated over the cell. Because the EHF at ϕ_H is positive in the Northern Hemisphere, the first term represents poleward heat transport. However, the original HH80 framework neglects both the EHF and adiabatic processes, effectively simplifying Eq. (9) to

$$0 = \int_0^{\phi_H} \eta \, d\phi. \tag{10}$$

Substituting $\eta(\phi) = \theta(\phi) - \theta_E(\phi)$ into Eq. (10) yields $\int_0^{\phi_H} \theta \, d\phi = \int_0^{\phi_H} \theta_E \, d\phi$, which is equivalent to the constraint of potential temperature conservation employed in HH80 [see Eq. (5)].

b. Extension of energy flux balance with baroclinic eddies

Moon and Wettlaufer (2025) extended HH80 to include baroclinic eddies. They utilized a planetary-scale heat equation that parameterizes synoptic-scale eddies via turbulent eddy diffusion (Moon et al. 2021). Since parameterized diffusion represents poleward heat transport due to eddies (Okubo and Levin 2001), the first term of Eq. (9), corresponding to EHF convergence, is not assumed to be zero.

In this study, we consider both EHF and adiabatic processes. Their combined contribution—i.e., the sum of the first and second terms in Eq. (9)—is referred to as the eddy-induced thermal process (ET):

$$\int_0^{\phi_H} \frac{\partial}{\partial \phi}\langle \overline{v'\theta'} \rangle d\phi + \int_0^{\phi_H} \langle \overline{Sw} \rangle d\phi = \mathrm{ET} = -\frac{1}{\tau}\int_0^{\phi_H} \eta \, d\phi. \tag{11}$$

The ET is related to the HCE through $\eta(\phi) = \theta(\phi) - \theta_E(\phi)$. By using Eqs. (3) and (4), we have

$$\eta(\phi) = \eta_{\mathrm{eq}} - \frac{1}{2R}\Delta_H \phi^4 + \Delta_H \phi^2, \tag{12}$$

where $\eta_{\mathrm{eq}} = \theta_{\mathrm{eq}} - [1 + (1/3)\Delta_H]$. Here, η_{eq} is the potential temperature anomaly at the equator, which is calculated as $\theta(0) - \theta_E(0)$. As in HH80, we must determine two unknowns: the temperature anomaly at the equator η_{eq} and the HCE latitude ϕ_H. To do this, two thermodynamic conditions are assumed. First, the anomalous potential temperature should be continuous at the HCE (ϕ_H), which is assumed to be zero in the HH80 model (see Fig. 1). When there is energy transfer from the HC to midlatitudes across the HCE, η is no longer zero but a positive value. Second, the energy flux is assumed to be balanced. Without baroclinic eddies, the anomalous thermodynamic energy (measured by η) should be conserved within the HC (black line in Fig. 1, which shows that the areas formed by the zero and η lines have opposite signs and cancel each other out to become zero). With baroclinic eddies, however, energy is transferred to the midlatitudes.

Mathematically, these two constraints are represented as follows:

$$\eta_{\phi_H} = \eta_{\mathrm{eq}} - \frac{1}{2R}\Delta_H \phi_H^4 + \Delta_H \phi_H^2, \tag{13}$$

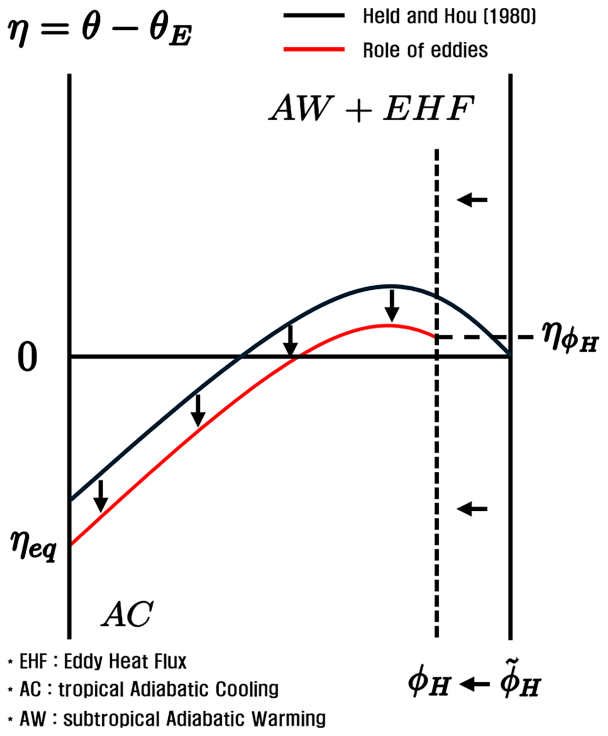

FIG. 1. A schematic illustrating the energy flux balance in the HC. The black line represents the energy flux balance in an eddy-free HC (HH80), where the domain-integrated anomalous potential temperature η is zero. The red line represents the energy flux balance in the present study, which includes the effects of baroclinic eddies. Here, η denotes the anomalous potential temperature relative to the RCE temperature. The η_{eq} and η_{ϕ} indicate the values of η at the equator and poleward HCE, respectively. The $\tilde{\phi}_H$ denotes the HCE in the original energy flux balance model, and ϕ_H is the HCE modified by the inclusion of baroclinic eddy effects.

$$-\tau\mathrm{ET} = \eta_{eq}\phi_H - \frac{1}{10R}\Delta_H\phi_H^5 + \frac{1}{3}\Delta_H\phi_H^3. \tag{14}$$

Combining the two equations yields

$$-\tau\mathrm{ET} = \eta_{\phi_H}\phi_H + \frac{2}{5R}\Delta_H\phi_H^5 - \frac{2}{3}\Delta_H\phi_H^3. \tag{15}$$

Next, we can express the HCE as $\phi_H = \tilde{\phi}_H + \phi_\eta$, where $\tilde{\phi}_H$ is the HCE without the effect of baroclinic eddies and ϕ_η is the perturbation due to baroclinic eddies. Assuming that radiative effects dominate over eddy effects at the HCE, $\tau\mathrm{ET} \ll 1$ is obtained. This indicates that the effect of baroclinic eddies is asymptotically small at the HCE, which leads to $\tilde{\phi}_H \gg \phi_\eta$. Using this approximation, Eq. (15) becomes

$$-\tau\mathrm{ET} \approx \eta_{\phi_H}\tilde{\phi}_H + \eta_{\phi_H}\phi_\eta + \frac{2}{5R}\Delta_H\tilde{\phi}_H^5 - \frac{2}{3}\Delta_H\tilde{\phi}_H^3 + \frac{2}{R}\Delta_H\tilde{\phi}_H^4\phi_\eta - 2\Delta_H\tilde{\phi}_H^2\phi_\eta, \tag{16}$$

where $\phi_H^5 \approx \tilde{\phi}_H^5 + 5\tilde{\phi}_H^4\phi_\eta$ and $\phi_H^3 \approx \tilde{\phi}_H^3 + 3\tilde{\phi}_H^2\phi_\eta$ are used. By neglecting the higher-order terms and separating the dominant and secondary terms, we arrive at

$$\begin{cases} \dfrac{2}{5R}\Delta_H\tilde{\phi}_H^5 - \dfrac{2}{3}\Delta_H\tilde{\phi}_H^3 = 0 \\ \dfrac{2}{R}\Delta_H\tilde{\phi}_H^4\phi_\eta - 2\Delta_H\tilde{\phi}_H^2\phi_\eta = -\tau\mathrm{ET} - \eta_{\phi_H}\tilde{\phi}_H. \end{cases} \tag{17}$$

Solving for ϕ_η, we obtain

$$\phi_\eta = -\frac{\tau\mathrm{ET} + \eta_{\phi_H}\tilde{\phi}_H}{\frac{2}{R}\Delta_H\tilde{\phi}_H^4 - 2\Delta_H\tilde{\phi}_H^2}. \tag{18}$$

Applying $\tilde{\phi}_H = \sqrt{(5/3)R}$, we obtain

$$\phi_H = \tilde{\phi}_H + \phi_\eta = \sqrt{\frac{5}{3}R} - \frac{\tau\mathrm{ET} + \eta_{\phi_H}\sqrt{\frac{5}{3}R}}{\frac{20}{9}\Delta_H R}. \tag{19}$$

This implies that as the ET decreases, the HCE (ϕ_H) expands. Importantly, η_{ϕ_H} has the same sign as ET because η_{ϕ_H} is induced by a nonzero ET (see Fig. 1).

Now, to calculate η_{eq}, Eq. (14) is approximated similarly:

$$-\tau\mathrm{ET} \approx \eta_{eq}\phi_H - \frac{1}{10R}(\tilde{\phi}_H^5 + 5\tilde{\phi}_H^4\phi_\eta) + \frac{1}{3}\Delta_H(\tilde{\phi}_H^3 + 3\tilde{\phi}_H^2\phi_\eta). \tag{20}$$

Applying $R = (3/5)\tilde{\phi}_H^2$, we obtain

$$-\tau\mathrm{ET} = \eta_{eq}\phi_H + \frac{1}{6}\Delta_H\tilde{\phi}_H^2(\widetilde{\phi_H} + \phi_\eta). \tag{21}$$

Then, rewriting $\tilde{\phi}_H^2 = (5/3)R$ and using $\phi_H = \widetilde{\phi_H} + \phi_\eta$, we derive

$$\eta_{eq} = -\frac{5}{18}\Delta_H R - \frac{\tau\mathrm{ET}}{\phi_H}. \tag{22}$$

This implies that the absolute magnitude of η_{eq} becomes larger owing to the presence of baroclinic eddies.

Notably, this approach differs from that of Moon and Wettlaufer (2025), who modeled the ET purely as eddy diffusion. The current study generalizes the influence of baroclinic eddies by considering both the EHF and adiabatic processes. Under quasigeostrophic theory, the zonal-mean vertical velocity is related to the EMF as follows:

$$\frac{1}{\rho_s}\frac{\partial\rho_s w}{\partial z} \propto -\frac{\partial^2}{\partial\phi^2}\langle\overline{u'v'}\rangle, \tag{23}$$

where ρ_s is the hemisphere-averaged density that depends only on height. This implies that the EMF in the upper subtropical troposphere modulates subtropical AW; in this way, AW is driven by the EMF. Finally, assuming no EHF at the equator, the total influence of baroclinic eddies on the HC ultimately manifests as three thermal processes: 1) EHF at the HCE, 2) AC in the tropics, and 3) AW in the subtropics. From Eq. (19),

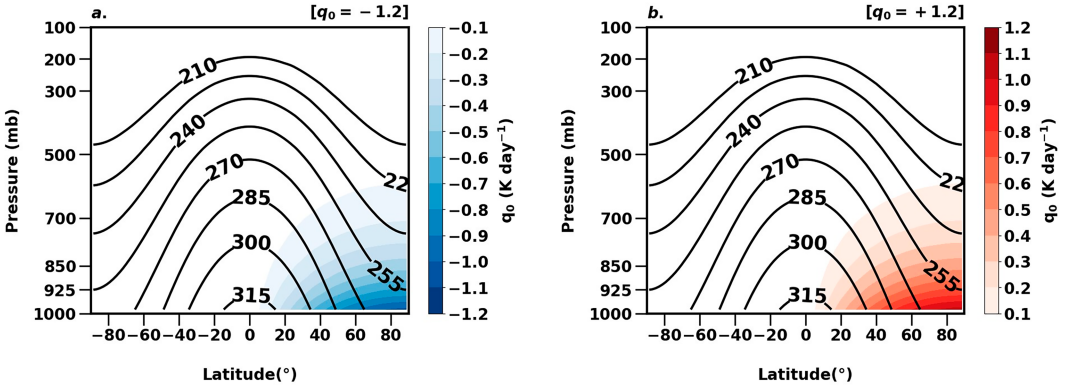

FIG. 2. Reference RCE temperature T_{ref} (black contours) and thermal forcing applied in the model experiment $\dot{T}$ (colors). The thermal forcing is designed to manipulate the meridional temperature gradient to induce differences in baroclinicity, with the forcing intensity q_0 ranging from ±1.2 K day^{-1} in increments of 0.3 K day^{-1}. The contour lines range from 315 to 210 K at 15-K intervals, and shading indicates forcing values from ±0.1 to ±1.2 K day^{-1} at 0.1 K day^{-1} intervals.

$$\Delta\phi_H \propto -\text{ET} = -\langle\overline{v'\theta'}\rangle|_{\phi_H} - \int_0^{\phi_c}\langle\overline{Sw}\rangle d\phi - \int_{\phi_c}^{\phi_H}\langle\overline{Sw}\rangle d\phi$$

$$\Delta\phi_H \propto -\text{EMF} - \text{AC} + \text{AW}, \tag{24}$$

where $\int_0^{\phi_H}\langle\overline{Sw}\rangle d\phi$ is decomposed into $\int_0^{\phi_c}\langle\overline{Sw}\rangle d\phi$ and $\int_{\phi_c}^{\phi_H}\langle\overline{Sw}\rangle d\phi$, which represent the tropical AC and subtropical AW, respectively. The ϕ_c denotes the latitude where AC transitions to AW within the HC. In the Northern Hemisphere, the EHF is positive at the HCE, and AC is positive, indicating that the first two terms on the right-hand side of Eq. (24) are negative, including a sign. In contrast, the last integral (vertical motion) is negative (i.e., downward), so this term (AW) becomes positive. To summarize, the EHF and AC are heat loss processes that contract the HC, whereas AW is a heat gain process that expands the HC. This finding is consistent with that of Moon and Wettlaufer (2025), who showed that the HCE contracts due to heat loss from interactions with baroclinic eddies.

Figure 1 illustrates the energy flux balance of the energetically isolated HH80 model (black line) and its updated state, including the new HCE and η_{eq}, when baroclinic eddies are considered (red line). Although baroclinic eddies have no direct effect at the equator, they indirectly influence tropical adiabatic cooling by modifying subtropical adiabatic warming through continuity. Thus, the energy flux balance of the HC is adjusted globally because of the influence of baroclinic eddies.

3. Data and methods

a. Model description and experimental design

A dry spectral dynamic core of the Geophysical Fluid Dynamics Laboratory (GFDL) Atmospheric Model, version 2 (AM2), was utilized in this study to verify the theoretical findings presented in Eq. (19). This model replaces radiation, turbulence, and convection processes with simplified forcing and dissipation schemes. Following Held and Suarez (1994), the temperature field is relaxed through Newtonian cooling toward a radiative equilibrium temperature profile T_{ref} with a specific response time scale:

$$T_{\text{ref}} = \max\left\{200\text{ K}, \left[315\text{ K} - \Delta_H \sin^2\phi - \Delta_v \log\left(\frac{p}{p_0}\right)\cos^2\phi\right]\left(\frac{p}{p_0}\right)^{R/C_p}\right\}. \tag{25}$$

Here, Δ_H is set to 60 K for the meridional temperature gradient and Δ_v is set to 10 K as the static stability parameter. The R/C_p is taken as 2/7. To mimic boundary layer friction, Reynolds damping is applied linearly to the zonal and meridional winds from the surface to $\sigma = 0.7$, with a diffusivity coefficient of $K_v = 0.5$. All other parameters are identical to those in Held and Suarez (1994). To analyze changes in the HCE in response to baroclinic eddies, as described in Eq. (19), baroclinicity is modulated by varying the meridional temperature gradient in T_{ref}. Following the approach of Butler et al. (2010) with minor modifications, an external thermal forcing term $\dot{T}$ is added as follows:

$$\dot{T} = q_0 \cos(\phi - \phi_0)\exp[6(P - P_0)], \tag{26}$$

where q_0 represents the intensity of the external thermal forcing. The ϕ_0 (=90°N) and P_0 (=1000 hPa) denote the central latitude and pressure of the prescribed thermal forcing, respectively. We conducted nine experimental simulations using different values of q_0, ranging from −1.2 to +1.2 K day^{-1}, in increments of 0.3 K day^{-1}. As shown in Fig. 2, the thermal forcing follows a cosine distribution from the pole to the equator in the Northern Hemisphere.

All experimental simulations were conducted at a T63 horizontal resolution with 20 vertical sigma levels, with seasonal variations and topographic effects not considered, as in Held and Suarez (1994). The analysis was performed over the final

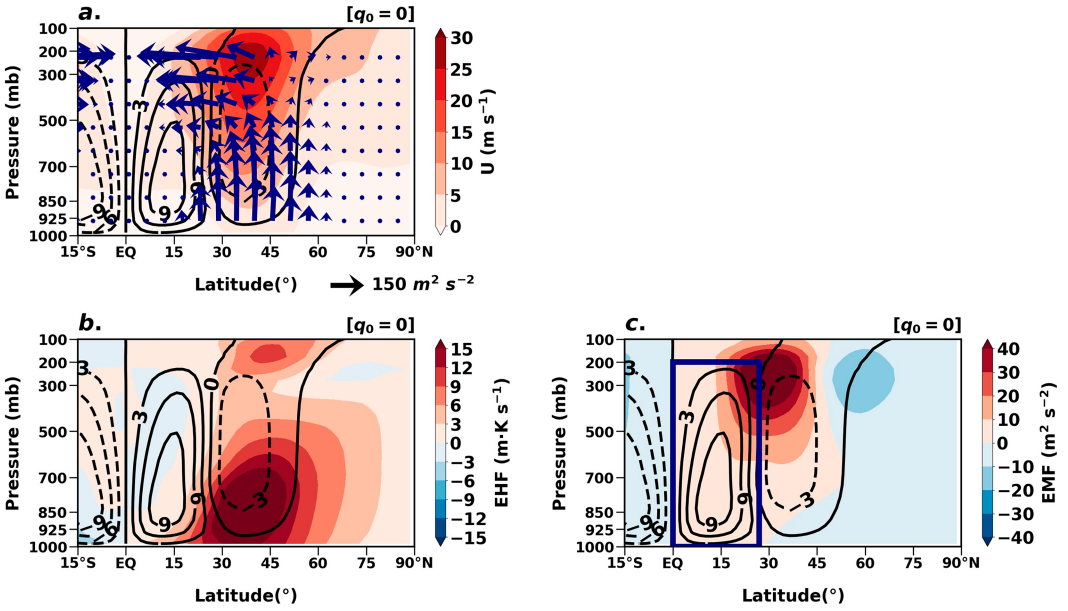

FIG. 3. Control run showing the mean meridional circulation (black contours) and (a) zonal wind, (b) EHF, and (c) EMF in color shading. The arrows in (a) indicate the EP flux, which represents the propagation of baroclinic eddies, scaled with a reference vector magnitude of 150 m^2 s^2. The navy box in (c) marks the HC domain used as a reference in this study. The contour units are 1010 kg s^{-1}.

4000 days of the 5000-day integration period, following a 1000-day spinup phase.

b. Definitions of variables

In the pressure and spherical coordinate system, with cosϕ approximated as 1 under the small-angle approximation, the ET is calculated as

$$\mathrm{ET} = \int_0^{\phi_H} \frac{\partial}{\partial \phi}\langle \overline{v'T'}\rangle d\phi - \int_0^{\phi_H} \langle \overline{S_p \omega}\rangle a\, d\phi. \qquad (27)$$

Here, ω represents the pressure velocity (Pa s^{-1}), and the dry static stability S_p is calculated as $(R_d T/C_p P) - (\partial T/\partial P)$. The R_d and C_p are set to 287 and 1004 J kg^{-1} K^{-1}, respectively. The vertical domain of the HC is defined from 1000 to 200 hPa for averaging.

To evaluate the HC edge and strength, we use the ψ metric. The mass streamfunction ψ is calculated as $\psi = (2\pi a \cos\phi/g)\int_0^P \overline{v}\, dp$. The HCE ($\phi_H$) is identified at 500 hPa, where ψ changes sign from positive to negative, and the strength ($\psi_{\max}$) is determined as the maximum value of ψ at 500 hPa within the HC domain (Seo et al. 2014; Adam et al. 2018).

The Eliassen–Palm (EP) flux is a diagnostic tool for visualizing the behavior of baroclinic eddies and is calculated as $\{F_\phi, F_p\} = \{-a\cos\phi \overline{u'v'}, fa\cos\phi(\overline{v'\theta'}/\theta_p)\}$ within a quasigeostrophic limit (Edmon et al. 1980). For visualization, it is scaled as $\{\widetilde{F_\phi}, \widetilde{F_p}\} = \{\cos\phi[(1/aF_\phi)/\pi], (F_p/10^5)\}$. This scaling ensures consistent units of meters per second squared (m^2 s^{-2}) between the horizontal and vertical components. To enhance the small vectors in the stratosphere, each component is further multiplied by $\sqrt{1000/p}$.

4. Results

a. Characteristics of baroclinic eddies

The meridional temperature gradient resulting from latitudinal thermal imbalances plays a crucial role in atmospheric dynamics. According to the thermal wind balance, this gradient induces vertical shear of the zonal-mean zonal wind, ultimately leading to a fluid-dynamic instability known as baroclinic instability. Midlatitude regions are characterized by significant vertical shear due to strong meridional temperature gradients. This is related to the intensity of jet streams in the upper atmosphere (Fig. 3a, color), which promote the growth and development of baroclinic eddies (Fig. 3a, arrows). Baroclinic eddies exhibit a clear life cycle from generation to dissipation. According to Simmons and Hoskins (1978), these eddies originate near the surface of baroclinically unstable regions, propagate upward and equatorward, and dissipate in the subtropical upper troposphere. This propagation can be visualized through the EP flux, represented by arrows in Fig. 3a. Baroclinic eddies grow by extracting energy from the mean field while dissipating through redistribution of that energy back to the mean field. The energy exchange between baroclinic eddies and the mean field is quantified through the EHF and EMF. EHF is primarily observed in the lower midlatitudes (Fig. 3b) and is closely associated with the growth and vertical propagation of baroclinic eddies. In contrast, the EMF is prominent in upper subtropical regions (Fig. 3c) and is closely related to the horizontal propagation and dissipation of baroclinic eddies. A positive EHF indicates poleward heat transport, implying that baroclinic eddies reduce latitudinal thermal imbalances. The dry spectral

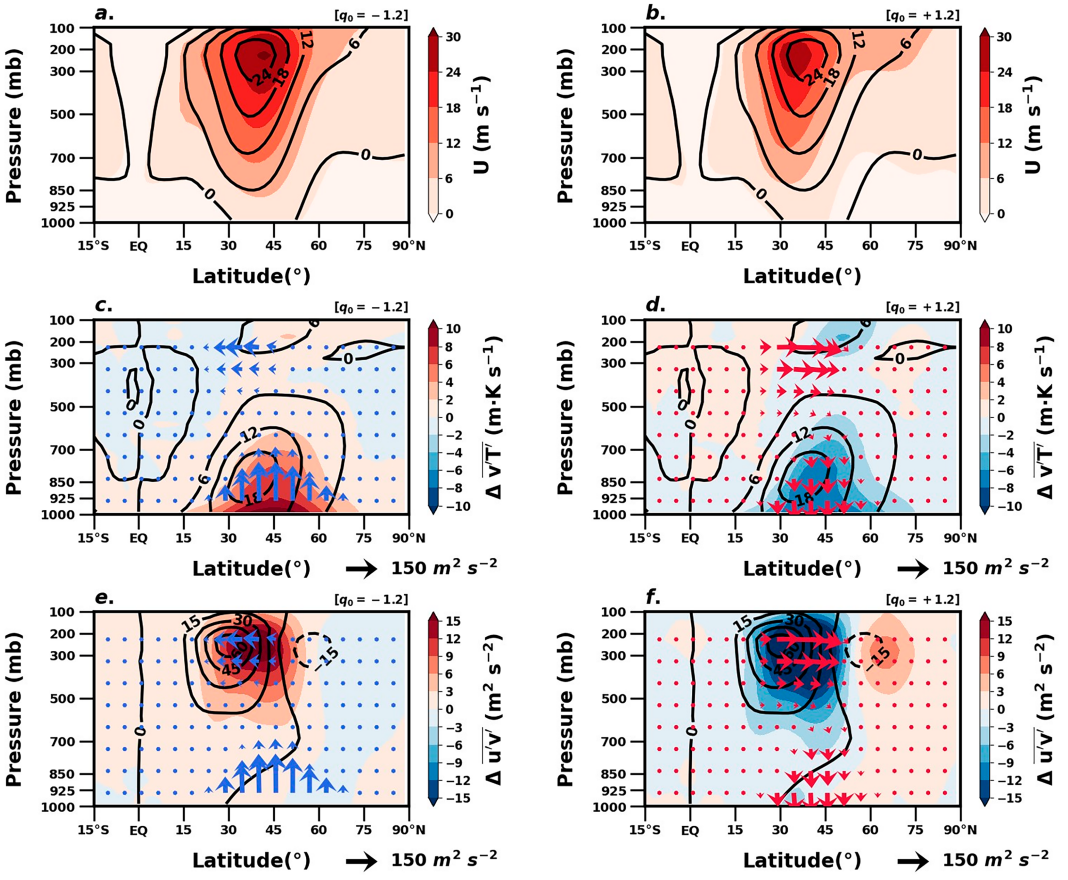

FIG. 4. Zonal-mean zonal wind and anomalies of heat and momentum flux and EP flux relative to the control run for (a),(c),(e) $q_0 = -1.2$ K day^{-1} and (b),(d),(f) $q_0 = +1.2$ K day^{-1} simulations. The contours in each panel represent values from the control run. The colors denote (a),(b) zonal-mean zonal wind, (c),(d) EHF anomalies, and (e),(f) EMF anomalies for each simulation. The arrows indicate EP flux anomalies, scaled with a reference vector magnitude of 150 m^2 s^2.

dynamic core model used in this study reproduces these typical features of baroclinic eddies (Fig. 3).

We prescribed various thermal forcings to the lower level of the Northern Hemisphere to implement different meridional temperature gradients in each simulation. Figure 4 shows the resulting baroclinicity in representative thermal forcing simulations of −1.2 and +1.2 K day^{-1}. Compared with the $q_o = -1.2$ K day^{-1} case, the $q_o = +1.2$ K day^{-1} simulation results in a relatively weaker meridional temperature gradient, thereby inducing weaker vertical shear. As a result, the $q_o = +1.2$ K day^{-1} simulation shows a relatively weak jet stream of approximately 24 m s^{-1} in the upper troposphere over the midlatitudes (Fig. 4b), whereas the $q_o = -1.2$ K day^{-1} simulation shows a strong jet stream of approximately 30 m s^{-1} (Fig. 4a). These changes in vertical shear result in differences in baroclinicity between the simulations. The arrows and shading in Figs. 4c–f represent the EP flux and eddy flux anomalies, respectively, relative to those in the control run. Compared with the control run, the $q_o = +1.2$ K day^{-1} simulation results in weaker baroclinic eddy activity (Figs. 4d,f), whereas the $q_o = -1.2$ K day^{-1} simulation results in stronger baroclinic eddy activity (Figs. 4c,e). Accordingly, the eddy fluxes $\overline{v'T'}$ (Figs. 4c,d) and $\overline{u'v'}$ (Figs. 4e,f), which are induced by energy exchange between baroclinic eddies and the mean field, are proportional to the intensity of baroclinicity in each experiment—showing larger values in the $q_o = -1.2$ K day^{-1} simulation and smaller values in the $q_o = +1.2$ K day^{-1} simulation. Consequently, as the thermal forcing increases from −1.2 to +1.2 K day^{-1} in the 0.3 K day^{-1} interval (the results from intermediate simulations are omitted), baroclinicity decreases nearly linearly because of the weakening of vertical shear caused by the reduction in the meridional temperature gradient. This leads to a corresponding weakening of baroclinic eddy activity and a decrease in eddy fluxes. The temperature response in the dry dynamic core model to the prescribed thermal forcing, as well as the resulting changes in eddy fluxes, is discussed in detail in Butler et al. (2010).

b. *Influence of baroclinic eddies on the HC*

The responses of the HCE (ϕ_H) and HC strength (ψ_{max}) across all the thermal forcing experiments conducted in this study are presented in Fig. 5.

We confirm that in the idealized dry model experiment, the HC simultaneously expands and strengthens (Fig. 5). This result is consistent with the reanalysis data, which show both

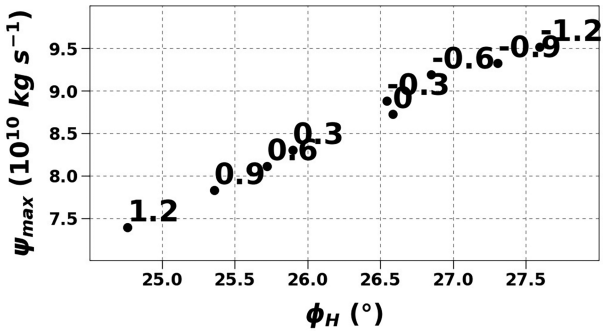

FIG. 5. Results of the HCE (ϕ_H) and HC strength ($\psi_{\max}$) in different thermal forcing experiments.

HC expansion (Hu and Fu 2007; Hu et al. 2018; Lucas et al. 2014; Johanson and Fu 2009) and intensification (Mitas and Clement 2005, 2006; Chemke and Polvani 2019; D'Agostino and Lionello 2017). In particular, Liu et al. (2012) identified a period from the late 1970s to the 2000s during which the HC exhibited both expansion and strengthening. However, studies using climate models have reported a weakening trend in HC intensity (Mitas and Clement 2006; Chemke and Polvani 2019). Therefore, the relationship between the HCE and its intensity remains an open question. While this topic remains under active discussion, Son et al. (2018) suggested that simultaneous HC expansion and strengthening can occur when the latitude of the upper-tropospheric EMF maximum shifts poleward and its intensity increases. In line with this, our study attempts to explain the co-occurrence of HC expansion and strengthening by incorporating key baroclinic eddy terms derived from the thermodynamic equation of the HH80 model.

According to Eq. (27), the relationship between the eddy-induced thermal processes in pressure coordinates and the HCE can be expressed as follows:

$$\Delta\phi_H \propto -\mathrm{ET} = -\overline{\langle v'T'\rangle}|_{\phi_H} + \int_0^{\phi_c} \langle \overline{S_p\omega}\rangle a\, d\phi + \int_{\phi_c}^{\phi_H} \langle \overline{S_p\omega}\rangle a\, d\phi. \tag{28}$$

First, $\overline{\langle v'T'\rangle}|_{\phi_H}$ represents the EHF at the HCE. As shown in Fig. 3b, the EHF is positive at ϕ_H in the Northern Hemisphere, indicating heat loss from the HC due to poleward heat transport by baroclinic eddies. Second, $\int_{\phi_c}^{\phi_H} \langle \overline{S_p\omega}\rangle a\, d\phi$ represents the subtropical AW. This is related to the fact that baroclinic eddies supply the EMF to the mean flow (Fig. 3c), typically in the mid- and upper troposphere, and the vertical gradient of upward motion is proportional to the EMF itself [Eq. (23)], modulating the subtropical AW within the HC. This downward motion in this region leads to heat gain. Third, $\int_0^{\phi_c} \langle \overline{S_p\omega}\rangle a\, d\phi$ represents the tropical AC, resulting in heat loss from the HC.

A quantitative assessment of these three processes is performed using the nine simulations with varying degrees of baroclinic eddy activity. The EMF is calculated by averaging over the region from ϕ_c to ϕ_H and from 200 to 500 hPa to capture the subtropical AW modulated by the EMF. As shown in Fig. 6a, the EHF and EMF both decrease linearly as the thermal forcing increases from -1.2 to $+1.2$ K day^{-1}, reflecting weakened baroclinic eddy activity due to reduced baroclinicity. The relationship between the tropical AC and subtropical AW is shown in Fig. 6c, where a reduced EMF leads to reduced AW, which, in turn, reduces AC. This aligns with previous studies showing that extratropical eddy fluxes can modulate tropical dynamics (Kim and Lee 2001).

A key observation in the idealized dry model experiment is that subtropical AW is greater and more variable than tropical AC (Fig. 6c). This likely results from the model's inability to fully capture strong vertical motions in the deep tropics, such as those associated with the intertropical convergence zone (ITCZ). Consequently, subtropical AW induced by baroclinic eddies plays a more dominant role than tropical AC in this model simulation.

Recall that AW contributes to HC expansion [Eq. (28)], and the EMF modulates vertical motion [Eq. (23)]. In the -1.2 K day^{-1} simulation—characterized by the strongest baroclinicity—the upper-level subtropical EMF is the largest, resulting in a significant increase in AW (Fig. 6b). This corresponds to stronger downward motion over the subtropical region and

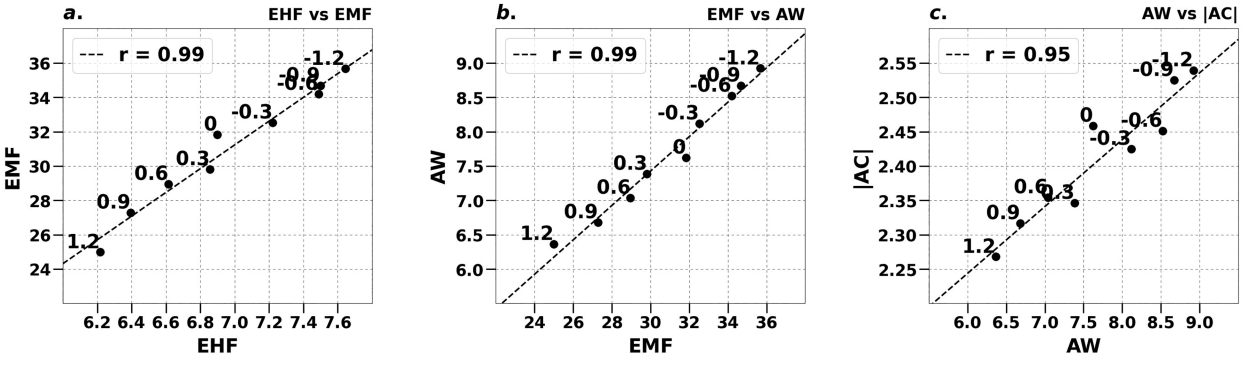

FIG. 6. Relationships among EHF, EMF, tropical AC, and subtropical warming (AW) among different thermal forcing experiments. The EHF is calculated as $\overline{\langle v'T'\rangle}|_{\phi_H}$, averaged from 200 to 1000 hPa. AC and AW are calculated as $\int_0^{\phi_c} \langle \overline{S_pW}\rangle a\, d\phi$ and $\int_{\phi_c}^{\phi_H} \langle \overline{S_pW}\rangle a\, d\phi$, respectively, and are averaged over 200–1000 hPa. (c) The tropical AC is obtained as the absolute value $|\int_0^{\phi_c} \langle \overline{S_pW}\rangle a\, d\phi|$. The EMF is averaged from ϕ_c to ϕ_H and from 200 to 500 hPa. The ϕ_c is defined as the latitude where $\langle \overline{S_pW}\rangle$ changes sign at 500 hPa within the HC. The dots represent different thermal forcing experiments, and the black dashed lines indicate linear regressions between the variables in each panel, with their correlation coefficients denoted as *r*.

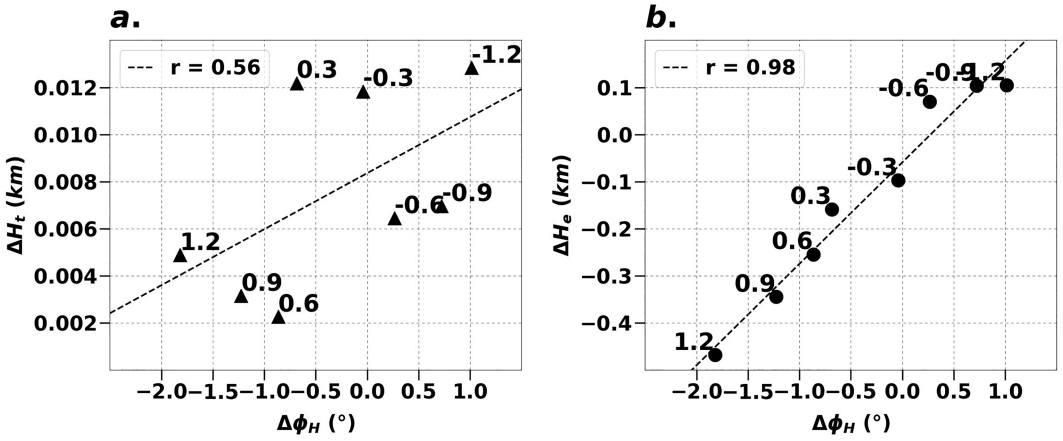

FIG. 7. Relationship between HC widening $\Delta\phi_H$ and changes in (a) tropical tropopause height ΔH_t and (b) extratropical tropopause height ΔH_e. The Δ denotes the anomaly, which is calculated as the difference between each experiment and the control run. The ϕ_H is defined as the latitude where the mass streamfunction ψ at 500 hPa crosses zero. The H_t is averaged over 20°S–20°N, and H_e is averaged over 35°–55°N. The black dashed lines indicate linear regressions between the variables in each panel, with their correlation coefficients denoted as r.

an intensification of the HC. However, in the idealized dry model, the response of AW to increasing EMF is much stronger than that of AC (Fig. 6c). In this way, HC expansion can occur concurrently with HC strengthening (Fig. 6). Thus, while not an identical mechanism, Eq. (28) supports the relationship between HC expansion and the strengthening discussed in Son et al. (2018), providing an interpretation from the perspective of baroclinic eddies.

Thus, the linear relationships among EHF, EMF, AW, and AC (Fig. 6) suggest that the influence of baroclinic eddies cannot be excluded from the perspective of the HC energy flux balance. In particular, the impact of baroclinic eddies is not only limited to the EHF but also emerges through the responses of the subtropical AW and tropical AC to variations in the EMF in the upper subtropical region.

c. *Scaling of the HC edge and strength*

HH80 scaled the HCE to the tropical tropopause height on the basis of the assumption of angular momentum conservation under inviscid conditions [Eq. (6)]. Later, an alternative scaling was proposed by H2000, which assumes that angular momentum is conserved only up to the region where baroclinic instability occurs. As a result, the HCE is scaled by the extratropical tropopause height and static stability [Eq. (7)].

Figure 7 illustrates the relationship between changes in tropical and extratropical tropopause heights and HC widening on the basis of various baroclinicity experiments conducted in this study. The tropopause height is defined as the lowest altitude at which the lapse rate decreases to 2 K km^{-1}. Following Lu et al. (2007), the tropical tropopause height is averaged over the latitudinal range of 20°S–20°N, and the extratropical tropopause height is averaged over 35°–55°N. As reported in previous studies, the extratropical tropopause height explains the HCE variability more effectively than the tropical tropopause height does (Lu et al. 2007). This indicates that the baroclinicity of the subtropical and extratropical regions plays a crucial role in understanding HC dynamics (Frierson et al. 2007; Levine and Schneider 2015; Kang and Lu 2012).

Next, we need to check how well the derived solution of ϕ_H [Eq. (19)] fits the model simulations. Figure 8a presents the theoretical estimate [Eq. (19)] with $g = 9.8$ m s^{-2}, $\Omega = 7.29 \times 10^{-5}$ rad s^{-1}, $a = 6.37$ km $\times$ 103 km, and $\tau = 40$ days. Since the actual equator-pole temperature gradient in the RCE Δ_H varies across experiments due to the addition of external thermal forcing q_0, it is difficult to directly compute this value. Instead, for simplicity and consistency, we assume that $\Delta_H = 60$ K is a constant and accordingly set $\theta_0 = 300$ K. The values of H_t, ET, and η_{ϕ_H} are computed for each experiment. The H_t is calculated as the average over 20°S–20°N, and ET is integrated from 0° to a fixed latitude of 27°N. This is because treating ϕ_H as an experiment-dependent value when calculating ET captures concurrent changes in the HCE and relevant physical quantities, potentially making the result appear to be a trivial consequence. To avoid such misinterpretation, we fix the integration boundary at 27°N, which is the closest to the control run HCE value considering the model resolution. The η_{ϕ_H}, defined as the difference between the resulting potential temperature and the RCE potential temperature, is averaged vertically at 27°N.

There is a discrepancy of approximately 2° between the model-simulated ϕ_H value and the theoretically estimated ϕ_{Est} (gray line representing $y = x$). This deviation arises because large-scale flow from the tropics to the subtropics does not perfectly conserve angular momentum (Walker and Schneider 2005, 2006); however, the first term on the right side of Eq. (19) comes from HH80. Additionally, identifying a sharp boundary between the HC and the midlatitude Ferrel cell is inherently difficult. Even when the meridional mass streamfunction is used, the diagnosed edge does not always align well vertically. Nonetheless, the theoretical estimation remains close to ϕ_H, and the variation between the model-derived HCE and the theoretically estimated HCE is consistent,

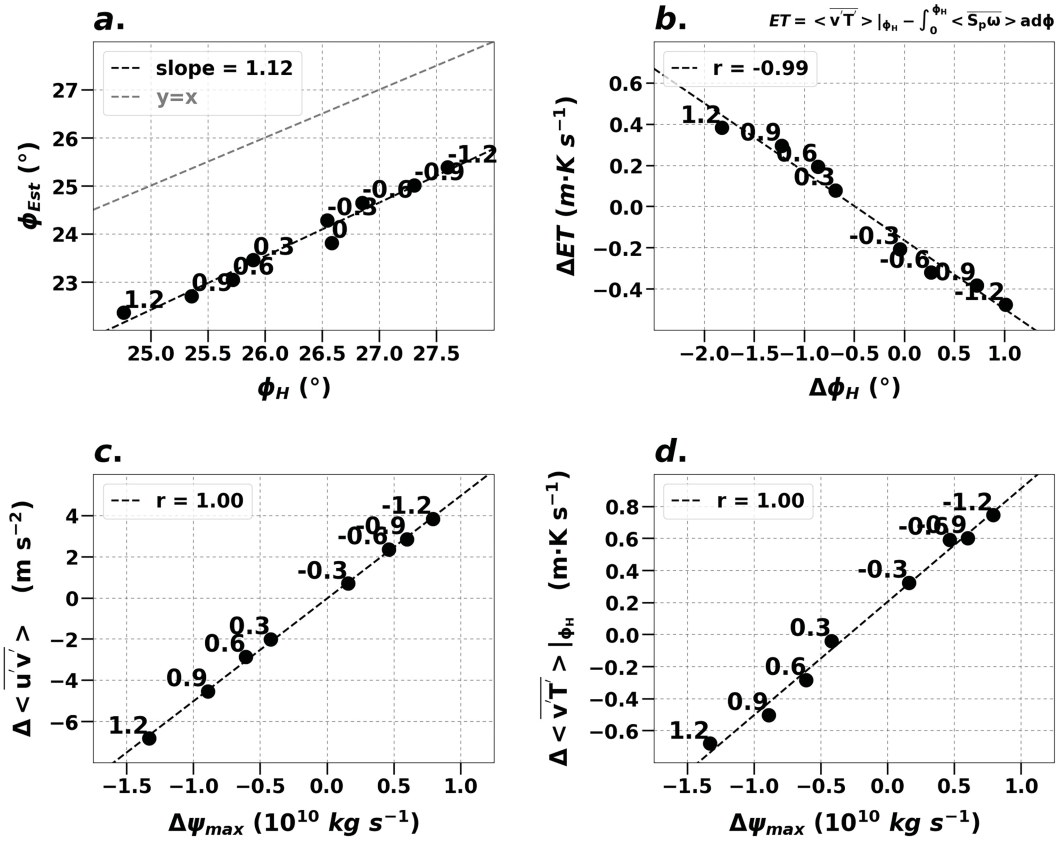

FIG. 8. Relationships between (a) HCE (ϕ_H) and the theoretical estimation of Eq. (19) ϕ_{Est}, (b) HC widening $\Delta\phi_H$ and changes in eddy-induced thermal processes ΔET, (c) changes in HC strength $\Delta\psi_{\max}$ and EMF, and (d) changes in HC strength $\Delta\psi_{\max}$ and EHF. The Δ denotes the anomaly, which is calculated as the difference between each experiment and the control run. The EMF is averaged from ϕ_c to ϕ_H, and from 200 to 500 hPa, the EHF is averaged from 200 to 1000 hPa at ϕ_H. The dots represent different thermal forcing experiments. The black dashed lines indicate linear regressions between the variables in each panel, with their correlation coefficients denoted as r.

with a slope of 1.12 (Fig. 8a). Importantly, this property supports the key argument that energy transport from the tropics to the midlatitudes via baroclinic eddies is closely linked to changes in the HCE and HC intensity.

The correlation coefficient between the HCE and ET for different baroclinicity experiments is −0.99 (Fig. 8b). Since a positive ΔET represents heat loss from the HC through interactions with baroclinic eddies, the negative correlation between $\Delta\phi_H$ and ΔET is consistent with the theoretical prediction of Eq. (19). In addition, we tested integration boundaries of 0°–25°N, 0°–29°N, and 0°–31°N for ET and found that the correlation coefficients between ΔET and $\Delta\phi_H$ were −0.97, −0.99, and −0.99, respectively (not shown). This finding indicates that the relationship between ΔET and $\Delta\phi_H$ in the dry model is not highly sensitive to the choice of integration boundary for the ET. In general, baroclinic instability increases gradually from the HCE to the jet center, where baroclinicity is strongest (Fig. 3). Therefore, the choice of integration boundaries within this range is considered to have only a minor impact on the relationship between ET and HCE. For example, when the integration boundary for the ET is extended poleward, AW increases gradually with increasing EHF. As a result, since the two variables are ultimately linearly coupled in Eq. (28), integration boundaries within this range consistently capture the influence of baroclinic eddies on the HCE. However, the ET should be defined within a domain that sufficiently reflects the internal energy of the HC. While a certain degree of flexibility in its definition is acceptable depending on the analytical purpose, shifting the integration boundary equatorward requires more caution.

The model simulations further indicate that energy transfer through the EHF, AC, and AW is tightly coupled with the life cycle of the baroclinic wave. Baroclinic instability near the surface initiates wave growth. The EHF is associated with the growth and upward propagation of waves, whereas the EMF is related to their equatorward propagation and dissipation in the upper subtropical troposphere. This upper-level EMF drives subsidence in the subtropics (and the resulting AW), contributing to the strengthening of the HC. The subsequent downward motion near the HCE induces a tropical upward motion of comparable magnitude, with consequences for AC. Considering both the dynamic and thermodynamic roles of

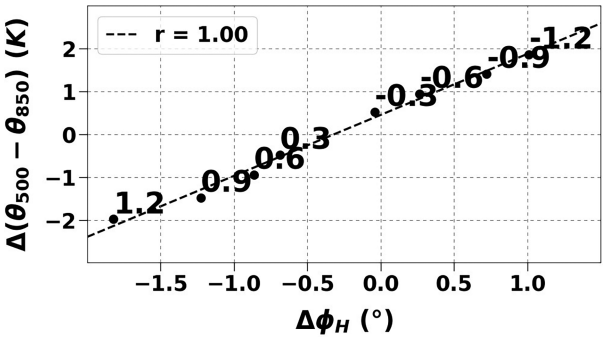

FIG. 9. Relationship between HC widening $\Delta\phi_H$ and change in the vertical gradient of potential temperature [$\Delta(\theta_{500} - \theta_{850})$], representing static stability. The gradient $\theta_{500} - \theta_{850}$ is calculated as the average from 15°N to the jet center at 40°N. The Δ denotes the anomaly obtained by subtracting the control run from each experiment.

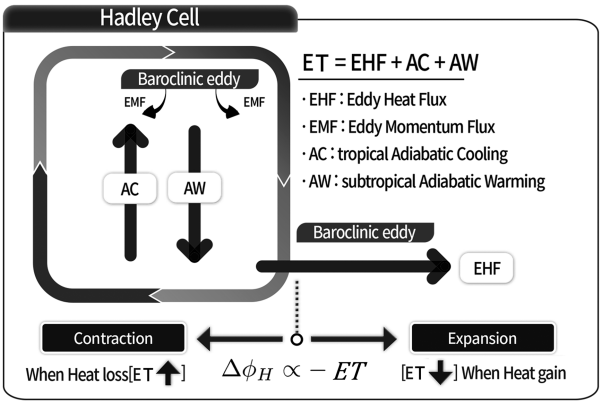

FIG. 10. Schematic diagram illustrating the thermal effects of baroclinic eddies on the HC. ET represents the eddy-induced thermal process as defined in this study. When the HC gains (loses) heat, it expands (contracts) because of thermal interchange with the baroclinic eddies.

baroclinic waves—from their generation to wave breaking—the EHF, AW, and AC are highly interrelated and can serve as robust metrics for scaling the overall strength of the HC (Figs. 8c,d).

d. Discussion

Subtropical static stability and vertical shear (or meridional temperature gradient) are also important for understanding the HC. These factors arise from the baroclinic instability criterion in H2000 and are consistent with previous studies that emphasized the role of subtropical influences on the HC (Lu et al. 2008; Son et al. 2018; Seo et al. 2023; Tandon et al. 2013).

In our idealized dry model with varying baroclinicity experiments, the variations in subtropical static stability closely account for changes in the HCE (Fig. 9). This tight coupling can be interpreted through baroclinic adjustment: In the absence of water vapor effects and under RCE conditions, bulk static stability increases in direct proportion to the meridional surface temperature gradient in the midlatitudes (??). Consequently, $q_o = -1.2$ K day^{-1} experiments with stronger meridional temperature gradients attain proportionally higher static stability and, via the H2000 scaling in Eq. (7), exhibit poleward displacement of the HCE (Fig. 9).

However, in moist atmospheres, water vapor and latent heat release affect static stability, so the relationship between baroclinicity and stability is not always linear (Seo et al. 2023). This limitation cautions against diagnosing the full influence of static stability on the HCE solely from dry experiments. ?? noted that including moist processes introduces additional dynamic and kinematic complexities because moisture actively regulates the mean state stability. Thus, although a dry framework clarifies the mechanistic link between baroclinic eddies and static stability, the presence of moisture can fundamentally reorganize this linkage.

In the present study, static stability can be considered a component of adiabatic processes. Specifically, the adiabatic process is expressed as the product of static stability S_p and vertical motion ω, expressed as $S_p\omega$. While we focus primarily on the physical effects of baroclinic eddies in this step, the role of static stability beyond the baroclinic framework warrants further investigation in future work.

5. Conclusions

This study extends the classic HH80 theory of the HC by incorporating the role of baroclinic eddies, which are not considered in the original framework. While Moon and Wettlaufer (2025) parameterized these effects as eddy diffusion, we introduce a new theoretical model that accounts for both eddy heat flux (EHF) at the HCE and adiabatic processes driven by eddy momentum flux (EMF) in the upper subtropical troposphere. The key result is that the HCE depends on whether the heat exported by baroclinic eddies increases or decreases.

Our analysis identifies three key processes governing the relationship between the HCE and baroclinic eddies:

1) EHF at the HCE: Poleward heat transport due to baroclinic eddies leads to heat loss and contraction of the HC.
2) Subtropical adiabatic warming (AW): EMF-induced descent results in increased subtropical AW, heat gain, and expansion of the HC.
3) Tropical adiabatic cooling (AC): To maintain energy flux balance within the HC, tropical AC intensifies in response to enhanced subtropical AW, causing heat loss and contraction of the HC.

Because these processes have opposing effects on HC expansion/contraction, a comprehensive consideration of their interactions is necessary. The relationship between the HC and baroclinic eddies is summarized schematically in Fig. 10.

These components form the eddy-induced thermal process (ET), which we introduce as a reliable predictor of HCE variability (with a correlation of −0.99). Using a dry dynamic core model with varying degrees of baroclinicity, we validate the theoretical predictions and confirm the strong linear relationships among EHF, EMF, AW, and AC (Fig. 6). The

derived HCE solution from our extended theory shows high consistency with the simulated HCE with slight degeneracy (i.e., a 2° HCE offset occurs, which derives from utilization of the angular momentum conservation framework). Our results demonstrate that baroclinic eddies influence not only the width of the HC but also its strength and highlight the need to explicitly incorporate eddy effects into the theoretical frameworks of large-scale tropical circulations.

Acknowledgments. This research was supported by the Basic Science Research Program through the National Research Foundation of Korea (NRF), funded by the Ministry of Education (RS-2023-00281017) and supported by the Global Learning & Academic Research Institution for Master's PhD students and the Postdocs (LAMP) Program of the National Research Foundation of Korea (NRF) grant funded by the Ministry of Education (RS-2023-00301702) and (RS-2023-00301938). KHS is also supported by the Korea Meteorological Administration (KMA) Research and Development Program under Grant RS-2024-00403698.

Data availability statement. For access to the data used in this study, please contact the corresponding author (woosok.moon@gmail.com).

REFERENCES

Adam, O., and Coauthors, 2018: The TropD software package (v1): Standardized methods for calculating tropical-width diagnostics. *Geosci. Model Dev.*, **11**, 4339–4357, https://doi.org/10.5194/gmd-11-4339-2018.

Becker, E., G. Schmitz, and R. Geprägs, 1997: The feedback of midlatitude waves onto the Hadley cell in a simple general circulation model. *Tellus*, **49A**, 182–199, https://doi.org/10.3402/tellusa.v49i2.14464.

Butler, A. H., D. W. J. Thompson, and R. Heikes, 2010: The steady-state atmospheric circulation response to climate change–like thermal forcings in a simple general circulation model. *J. Climate*, **23**, 3474–3496, https://doi.org/10.1175/2010JCLI3228.1.

Chemke, R., and L. M. Polvani, 2019: Opposite tropical circulation trends in climate models and in reanalyses. *Nat. Geosci.*, **12**, 528–532, https://doi.org/10.1038/s41561-019-0383-x.

D'Agostino, R., and P. Lionello, 2017: Evidence of global warming impact on the evolution of the Hadley Circulation in ECMWF centennial reanalyses. *Climate Dyn.*, **48**, 3047–3060, https://doi.org/10.1007/s00382-016-3250-0.

Edmon, H. J., Jr., B. J. Hoskins, and M. E. McIntyre, 1980: Eliassen-palm cross sections for the troposphere. *J. Atmos. Sci.*, **37**, 2600–2616, https://doi.org/10.1175/1520-0469(1980)037<2600:EPCSFT>2.0.CO;2.

Feng, S., and Q. Fu, 2013: Expansion of global drylands under a warming climate. *Atmos. Chem. Phys.*, **13**, 10 081–10 094, https://doi.org/10.5194/acp-13-10081-2013.

Frierson, D. M. W., J. Lu, and G. Chen, 2007: Width of the Hadley cell in simple and comprehensive general circulation models. *Geophys. Res. Lett.*, **34**, L18804, https://doi.org/10.1029/2007GL031115.

Fu, Q., C. M. Johanson, J. M. Wallace, and T. Reichler, 2006: Enhanced mid-latitude tropospheric warming in satellite measurements. *Science*, **312**, 1179, https://doi.org/10.1126/science.1125566.

Grise, K. M., and S. M. Davis, 2020: Hadley cell expansion in CMIP6 models. *Atmos. Chem. Phys.*, **20**, 5249–5268, https://doi.org/10.5194/acp-20-5249-2020.

Held, I., 2000: The general circulation of the atmosphere, 2000 program of study in geophysical fluid dynamics. Woods Hole Oceanographic Institution Tech. Rep., 1 pp., https://gfd.whoi.edu/wp-content/uploads/sites/18/2018/07/previous_announcement2000_16868.pdf.

Held, I. M., and A. Y. Hou, 1980: Nonlinear axially symmetric circulations in a nearly inviscid atmosphere. *J. Atmos. Sci.*, **37**, 515–533, https://doi.org/10.1175/1520-0469(1980)037<0515:NASCIA>2.0.CO;2.

——, and M. J. Suarez, 1994: A proposal for the intercomparison of the dynamical cores of atmospheric general circulation models. *Bull. Amer. Meteor. Soc.*, **75**, 1825–1830, https://doi.org/10.1175/1520-0477(1994)075<1825:APFTIO>2.0.CO;2.

Hu, Y., and Q. Fu, 2007: Observed poleward expansion of the Hadley circulation since 1979. *Atmos. Chem. Phys.*, **7**, 5229–5236, https://doi.org/10.5194/acp-7-5229-2007.

——, H. Huang, and C. Zhou, 2018: Widening and weakening of the Hadley circulation under global warming. *Sci. Bull.*, **63**, 640–644, https://doi.org/10.1016/j.scib.2018.04.020.

Johanson, C. M., and Q. Fu, 2009: Hadley cell widening: Model simulations versus observations. *J. Climate*, **22**, 2713–2725, https://doi.org/10.1175/2008JCLI2620.1.

Kang, S. M., and J. Lu, 2012: Expansion of the Hadley cell under global warming: Winter versus summer. *J. Climate*, **25**, 8387–8393, https://doi.org/10.1175/JCLI-D-12-00323.1.

Kim, H.-K., and S. Lee, 2001: Hadley cell dynamics in a primitive equation model. Part II: Nonaxisymmetric flow. *J. Atmos. Sci.*, **58**, 2859–2871, https://doi.org/10.1175/1520-0469(2001)058<2859:HCDIAP>2.0.CO;2.

Kim, S.-Y., and S.-W. Son, 2020: Breakdown of the linear relationship between the Southern Hemisphere Hadley cell edge and jet latitude changes in the Last Glacial Maximum. *J. Climate*, **33**, 5713–5725, https://doi.org/10.1175/JCLI-D-19-0531.1.

——, and Coauthors, 2023: Hemispherically asymmetric Hadley cell response to CO_2 removal. *Sci. Adv.*, **9**, eadg1801, https://doi.org/10.1126/sciadv.adg1801.

Korty, R. L., and T. Schneider, 2008: Extent of Hadley circulations in dry atmospheres. *Geophys. Res. Lett.*, **35**, L23803, https://doi.org/10.1029/2008GL035847.

Levine, X. J., and T. Schneider, 2015: Baroclinic eddies and the extent of the Hadley circulation: An idealized GCM study. *J. Atmos. Sci.*, **72**, 2744–2761, https://doi.org/10.1175/JAS-D-14-0152.1.

Liu, J., M. Song, Y. Hu, and X. Ren, 2012: Changes in the strength and width of the Hadley circulation since 1871. *Climate Past*, **8**, 1169–1175, https://doi.org/10.5194/cp-8-1169-2012.

Lu, J., G. A. Vecchi, and T. Reichler, 2007: Expansion of the Hadley cell under global warming. *Geophys. Res. Lett.*, **34**, L06805, https://doi.org/10.1029/2006GL028443.

——, G. Chen, and D. M. W. Frierson, 2008: Response of the zonal mean atmospheric circulation to El Niño versus global warming. *J. Climate*, **21**, 5835–5851, https://doi.org/10.1175/2008JCLI2200.1.

Lucas, C., B. Timbal, and H. Nguyen, 2014: The expanding tropics: A critical assessment of the observational and modeling studies. *Wiley Interdiscip. Rev.: Climate Change*, **5**, 89–112, https://doi.org/10.1002/wcc.251.

Mitas, C. M., and A. Clement, 2005: Has the Hadley cell been strengthening in recent decades? *Geophys. Res. Lett.*, **32**, L03809, https://doi.org/10.1029/2004GL021765.

——, and ——, 2006: Recent behavior of the Hadley cell and tropical thermodynamics in climate models and reanalyses. *Geophys. Res. Lett.*, **33**, L01810, https://doi.org/10.1029/2005GL024406.

Moon, W., and J. S. Wettlaufer, 2025: Midlatitude interactions expand the Hadley circulation. *J. Atmos. Sci.*, **82**, 1057–1071, https://doi.org/10.1175/JAS-D-24-0099.1.

——, G. E. Manucharyan, and H. A. Dijkstra, 2021: Eddy memory as an explanation of intraseasonal periodic behaviour in baroclinic eddies. *Quart. J. Roy. Meteor. Soc.*, **147**, 2395–2408, https://doi.org/10.1002/qj.4030.

Nguyen, H., A. Evans, C. Lucas, I. Smith, and B. Timbal, 2013: The Hadley circulation in reanalyses: Climatology, variability, and change. *J. Climate*, **26**, 3357–3376, https://doi.org/10.1175/JCLI-D-12-00224.1.

——, C. Lucas, A. Evans, B. Timbal, and L. Hanson, 2015: Expansion of the Southern Hemisphere Hadley cell in response to greenhouse gas forcing. *J. Climate*, **28**, 8067–8077, https://doi.org/10.1175/JCLI-D-15-0139.1.

Okubo, A., and S. A. Levin, 2001: *Diffusion and Ecological Problems: Modern Perspectives.* Vol. 14, Springer, 468 pp.

Phillips, N. A., 1954: Energy transformations and meridional circulations associated with simple baroclinic waves in a two-level, quasi-geostrophic model. *Tellus*, **6** (3), 273–286, https://doi.org/10.3402/tellusa.v6i3.8734.

Rao, V. B., S. H. Franchito, M. B. Rosa, D. Govardhan, S. N. Figueroa, and V. S. L. Bhargavi, 2022: In a changing climate Hadley cell induces a record flood in Amazon and another recorded drought across South Brazil in 2021. *Nat. Hazards* , **114**, 1549–1561, https://doi.org/10.1007/s11069-022-05437-1.

Schmidt, D. F., and K. M. Grise, 2017: The response of local precipitation and sea level pressure to Hadley cell expansion. *Geophys. Res. Lett.*, **44**, 10573–10582, https://doi.org/10.1002/2017GL075380.

Schneider, E. K., 1977: Axially symmetric steady-state models of the basic state for instability and climate studies. Part II. Nonlinear calculations. *J. Atmos. Sci.*, **34**, 280–296, https://doi.org/10.1175/1520-0469(1977)034<0280:ASSSMO>2.0.CO;2.

Seo, K.-H., D. M. Frierson, and J.-H. Son, 2014: A mechanism for future changes in Hadley circulation strength in CMIP5 climate change simulations. *Geophys. Res. Lett.*, **41**, 5251–5258, https://doi.org/10.1002/2014GL060868.

——, S.-P. Yoon, J. Lu, Y. Hu, P. W. Staten, and D. M. Frierson, 2023: What controls the interannual variation of Hadley cell extent in the Northern Hemisphere: Physical mechanism and empirical model for edge variation. *npj Climate Atmos. Sci.*, **6**, 204, https://doi.org/10.1038/s41612-023-00533-w.

Simmons, A. J., and B. J. Hoskins, 1978: The life cycles of some nonlinear baroclinic waves. *J. Atmos. Sci.*, **35**, 414–432, https://doi.org/10.1175/1520-0469(1978)035<0414:TLCOSN>2.0.CO;2.

Son, S.-W., S.-Y. Kim, and S.-K. Min, 2018: Widening of the Hadley cell from Last Glacial Maximum to future climate. *J. Climate*, **31**, 267–281, https://doi.org/10.1175/JCLI-D-17-0328.1.

Studholme, J., A. V. Fedorov, S. K. Gulev, K. Emanuel, and K. Hodges, 2022: Poleward expansion of tropical cyclone latitudes in warming climates. *Nat. Geosci.*, **15**, 14–28, https://doi.org/10.1038/s41561-021-00859-1.

Tandon, N. F., E. P. Gerber, A. H. Sobel, and L. M. Polvani, 2013: Understanding Hadley cell expansion versus contraction: Insights from simplified models and implications for recent observations. *J. Climate*, **26**, 4304–4321, https://doi.org/10.1175/JCLI-D-12-00598.1.

Walker, C. C., and T. Schneider, 2005: Response of idealized Hadley circulations to seasonally varying heating. *Geophys. Res. Lett.*, **32**, L06813, https://doi.org/10.1029/2004GL022304.

——, and ——, 2006: Eddy influences on Hadley circulations: Simulations with an idealized GCM. *J. Atmos. Sci.*, **63**, 3333–3350, https://doi.org/10.1175/JAS3821.1.

Watt-Meyer, O., D. M. W. Frierson, and Q. Fu, 2019: Hemispheric asymmetry of tropical expansion under CO_2 forcing. *Geophys. Res. Lett.*, **46**, 9231–9240, https://doi.org/10.1029/2019GL083695.